Applied Surface Science 503 (2020) 144310

Contents lists available at ScienceDirect

Applied Surface Science

journal homepage: www.elsevier.com/locate/apsusc

Full Length Article

Influence of deposition temperature on the structure, optical and electrical properties of a-C films by DCMS

Hao Li[a], Peng Guo[a,*], Dong Zhang[a], Rende Chen[a], Xiao Zuo[a], Peiling Ke[a,b], Hidetoshi Saito[a,c], Aiying Wang[a,b,*]

[a] Key Laboratory of Marine Materials and Related Technologies, Zhejiang Key Laboratory of Marine Materials and Protective Technologies, Ningbo Institute of Materials Technology and Engineering, Chinese Academy of Sciences, 315201 Ningbo, PR China
[b] Center of Materials Science and Optoelectronics Engineering, University of Chinese Academy of Sciences, 100049 Beijing, PR China
[c] Graduate School of Engineering, Nagaoka University of Technology, 940-2188 Nagaoka, Japan

ARTICLE INFO

Keywords:
Amorphous carbon
Deposition temperature
Magnetron sputter
Opto-electrical property

ABSTRACT

Amorphous carbon films have been considered as strongly promising semiconductor materials, due to their superior mechanical properties, specific bond structures, as well as facile deposition over large area with device integrated processes. To figure out the effect of sp^2/sp^3 ratio and size of sp^2 clusters on opto-electrical behavior, we fabricated a series of H-free amorphous carbon (a-C) films by magnetron sputtering with a controllable deposition temperature from 30 to 400 °C. Result showed that all the films displayed a strong light absorption in the ultraviolet and visible regions, where the transmittance was less than 5% in the wavelength range of 200–750 nm, demonstrating the typical semiconductor behavior in temperature from 5 to 350 K, exhibiting a lower resistivity at higher temperature. In addition, their transmittance, optical bandgap, resistivity and activation energy showed similar tendency with increasing deposition temperature, which was discussed in terms of the evolution of sp^2/sp^3 ratio and sp^2 cluster in the a-C films. These studies provide a new route to tune optical and electrical properties of a-C films for their opto-electrical applications.

1. Introduction

Amorphous carbon (a-C) films with specific atomic bond structures have been widely used in various areas as protective and multifunctional materials on account of their outstanding mechanical and tribological properties, such as high hardness, low coefficient of friction and good chemical inertness [1–5]. Furthermore, as amorphous semiconductor materials, their resistivity can span in a wide range from 10^2 to 1016 ohm·cm [6], the optical band gap can also be adjusted at 0.8–4.0 eV, which is strongly dependent upon the deposition conditions. Very recently, a-C films have shown great potential in the field of optoelectronic devices, such as piezoresistive sensors, field emission cathodes, infrared detecting and optical windows [7–10].

To meet the highly demanded opto-electrical applications, however, it is still an opening challenge to figure out the main factors affecting opto-electrical properties of a-C films. For example, Dai and co-workers reported that both the sp^3 and sp^2 hybrid bonds dominated the opto-electrical properties of a-C films, since the optical bandgap and electrical resistivity were positively correlated with the ratio of sp^2/sp^3 bonds [11]. Besides, Mohagheghpour et al. pointed out that the electrical properties of a-C films showed the strong dependence on the size and distribution of sp^2 clusters [12]. Meanwhile, Caro et al. presented a computational study of tetrahedral amorphous carbon surfaces within density functional theory [13–15]. They considered the degree of localization of the electronic states was obtained with a participation ratio analysis, showing a direct relation with density and sp^2 fraction. In addition, Sze and co-workers demonstrated that the optical bandgap of a-C films deposited by plasma immersion ion implantation (PIII) decreased with increasing substrate bias voltage, due to the graphitizing of the a-C films [16]. Furthermore, Guo et al. observed the carrier transport of a-C was dominated by the thermally activated process with an activation energy of 0.1576 eV in the temperature range of 160–400 K [7,17]. Based on the previous studies, at least three factors will determine the opto-electrical properties of a-C films, namely, sp^2/sp^3 ratio, size and distribution of sp^2 clusters. While, considering the complexity of atomic structures and variety of deposition methods, the relationship between composition, structure and opto-electrical properties of a-C films were still diverse, especially in consideration of

* Corresponding authors at: Key Laboratory of Marine Materials and Related Technologies, Zhejiang Key Laboratory of Marine Materials and Protective Technologies, Ningbo Institute of Materials Technology and Engineering, Chinese Academy of Sciences, 315201 Ningbo, PR China (P. Guo & A. Wang).
E-mail addresses: guopeng@nimte.ac.cn (P. Guo), aywang@nimte.ac.cn (A. Wang).

https://doi.org/10.1016/j.apsusc.2019.144310
Received 18 July 2019; Received in revised form 1 September 2019; Accepted 6 October 2019
Available online 23 October 2019
0169-4332/

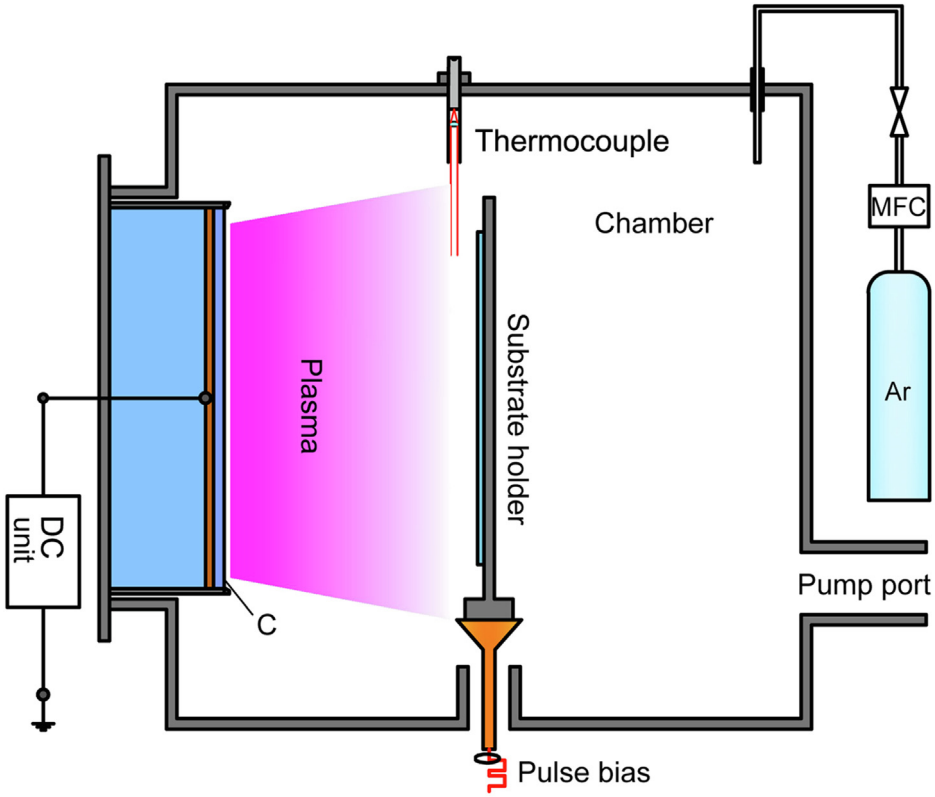

Fig. 1. A schematic diagram of DCMS equipment.

designing high-performance carbon-based optoelectronic devices [18].

In this study, H-free a-C films were selected and prepared by direct current magnetron sputter (DCMS) technique. The composition and structure of a-C films were adjusted by changing deposition temperature from 30 to 400 °C. The dependence of sp^2/sp^3 ratio and sp^2 clusters on the opto-electrical properties of a-C films was systematically studied.

2. Experimental details

The a-C films were deposited by DCMS (P600-1) with a supplied graphite target (380 mm × 100 mm × 7 mm) of 99.99% purity, as shown in Fig. 1 [19]. The P type Si (1 0 0) wafer, quartz and Al_2O_3 (0 0 0 1) were used as substrates. The substrates were cleaned step by step in ultrasonic bath of acetone and alcohol, respectively, before loaded into the deposition chamber. When the chamber vacuum (background vacuum) reached 3×10^{-3} Pa, all the substrates were cleaned by Ar^+ glow discharge at a bias of −350 V for 30 min. During deposition, the power of DC magnetron sputtering was kept at 1.7 kW, that was the power density was about 4.47 W/cm^2, with negative DC bias −300 V. The thicknesses of all the a-C films were maintained at around 190 ± 30 nm by changing the deposition time.

The thickness of the as-deposited a-C films was examined by a surface profilometer (Alpha-Step IQ, US), with employing a step formed by a shadow mask. The surface topography and surface roughness of the a-C films were measured by a Scanning Probe Microscope (Dimension 3100 V, Veeco, US), and the atomic force microscopy (AFM) analyses were performed on a tapping mode with scan rate of 2.0 Hz. Root-mean-square roughness (Rq) of the a-C films was calculated from 512 × 512 surface height data points obtained from the 3 μm × 3 μm scan area with NanoScope Analysis 1.5 software.

The chemical composition of the a-C films was investigated by X-ray photoelectron spectroscopy (XPS, Axis ultradld, Japan) with monochromated Al (mono) Kα irradiation at a pass energy of 160 eV, the analyzed area was cleaned by Ar^+ ions of 2 keV for 3 min before measurement in order to remove surface contamination. Here, the sp^2 contents in the a-C films were determined from the C 1s XPS spectra, with a mixture of a Gaussian (20%) and a Lorentzian (80%) function used to fit the sp^2-C peak and sp^3-C peak after a Shirley background subtraction [20–22]. The atomic bonding structure of the films was characterized by a Raman spectroscopy (Renishaw in Via-reflex, 532 nm) at a detecting range from 800 to 2000 cm^{-1}. The microstructure of the a-C film deposited at room temperature was examined by high-resolution transmission electron microscopy (TEM, Tecnai F20, US) with operating voltage 200 kV, and the sample for TEM observation was prepared with Focused Ion Beam (FIB) instrument (Carl Zeiss, Auriga)

The transmittance of the deposited a-C films was tested by Fourier transformation infrared spectrum (FTIR, Thermo, US) in the wavelength range from 2.5 to 15 μm, with a resolution of 1 cm^{-1} and scanning wavenumber range from 400 to 2000 cm^{-1}, and ultraviolet–visible spectrophotometer (Lambda 950, US) in the wavelength range from 15 to 25 μm, with scanning step size 1 nm. And the samples for transmittance test were deposited on quartz substrates [23,24]. The room temperature resistivity, current-voltage (I-V) feature of the samples were measured by Hall-effect measurement (Nanometrics, HP-5500C, US). The temperature dependence of dark electrical resistivity (ρ) of the a-C films was tested by physical property measurement system (PPMS, Quantum Design, Model-9) in a standard 4-probe way along with the temperature range of 5–350 K.

3. Result and discussion

3.1. Thickness and morphology

The thickness and deposition rate of a-C films prepared at various temperature are listed in Table 1. As the deposition temperature increased from 30 °C to 400 °C, the thickness of a-C films increased from 162 nm to 219 nm, with the corresponding deposition rate increasing

Table 1
The thickness, average deposition rate and Rq of the a-C films at various temperatures.

Temperature (°C)	Thickness (nm)	Deposition Rate (nm/min)	Rq (nm)
30	162	5.4	0.4
100	153	5.11	2.7
200	175	5.84	3.4
300	208	6.93	3.0
400	219	7.3	6.0

mildly from 5.4 nm/min to 7.3 nm/min, because the surface bonding force between carbon particles and the substrate increased with increasing deposition temperature when the deposition temperature was below 400 °C [25–29].

The tapping mode 2D-AFM images and the corresponding 3D-AFM images of the films at different temperature are shown in Fig. 2. Overall, all the a-C films showed continuous, uniform and smooth surfaces, despite the surfaces became rough slightly with elevated temperature, where the Rq increased from 0.4 nm at 30 °C to 6.0 nm at 400 °C, as illustrated in Table 1. The evolution of the surface morphology could be explained from the diffusion process during deposition of a-C films, in which the carbon atoms adsorbed onto the surface attempted to gather into many clusters, resulting in a rougher surface at higher deposition temperature [28].

3.2. Chemical composition and structure

Fig. 3(a) demonstrates the influence of deposition temperature on the full XPS spectra at various deposition temperatures. All the a-C films were mainly composed of two elements C and O, the small amount of O element might come from the residual oxygen in the vacuum chamber during deposition and the oxygen absorbed by a-C film exposed in the air [29,30]. The XPS C 1s spectra (Inserts in Fig. 3(b)) were fitted into three dominant peaks approximately centered at 284.6 eV, 285.4 eV, 286.6 eV, corresponding to sp^2, sp^3, and C—O/C═O hybridization, respectively [12,22,29,30]. By integrating the peak area, sp^2 and sp^3 carbon hybridization ratio could be deduced as shown in Fig. 3(b). With increasing deposition temperature from 30 °C to 400 °C, the sp^2 content of a-C films increased from around 59% to 70%, implying that the C atoms in the films tended to form stable sp^2 phases at higher temperature and higher growth rates [12,21,31,32].

The Raman spectra of a-C films deposited at various temperatures on silicon substrates in the range from 800 to 2000 cm^{-1} are shown in Fig. 4(a). In order to obtain the bond arrangements, furthermore, Raman spectra were fitted by two Gaussian peaks after a linear background subtraction [33–36]. Generally, G and D peaks are attributed to the vibration of sp^2 bonded carbon atoms [12], the G peak origins from the stretching vibration of sp^2 atoms in rings and chains, while D peak results from sp^2 atoms only in rings. The fitted G peak position, peak area ratio I_D/I_G and half maximum of G-peak (G FWHM) values, as shown in Fig. 4(b), can reflect carbon atoms disorder degrees, sp^2/sp^3 ratio, sp^2 cluster size and so on [37]. With the temperature changing from 30 °C to 400 °C, the G peak position shifted upward obviously from 1550 cm^{-1} to 1578 cm^{-1}, which implied the increase of sp^2 contents [34,38,39] and coincided with the former XPS results. According to the cluster modes of amorphous carbon [34], all a-C films were in the transitional stage from amorphous carbon (G peak ~1510 cm^{-1}) to nanocrystalline graphite (nc-G) (G peak ~1600 cm^{-1}). In addition, the G FWHM decreased evidently from 171.5 to 134 cm^{-1}, indicating that the structure of a-C matrix became much more ordered; on the contrary, the I_D/I_G increased from its minimum value around 2.67 at 30 °C to its maximum value 4.25 at 400 °C. It could be inferred that the average size of sp^2 clusters decreased with increasing deposition temperature, since I_D/I_G varies inversely with the in-plane correlation length La in the transitional stage from amorphous carbon to nc-G [40].

In order to observe the microstructure of the a-C films directly, the typical cross-sectional TEM image, high resolution transmission electron microscopy (HRTEM) and the corresponding selected area electron diffraction (SAED) pattern of the typical a-C film deposited at 100 °C are displayed in Fig. 5(a) and (b). Apparently, the thickness of a-C film was around 200 nm and all the films exhibited a compact, uniform and fine cross-sectional morphology, and no nanocrystalline can be observed, as shown in Fig. 5(a). The corresponding SAED pattern just presented a weak diffuse halo, as shown in Fig. 5(b), which indicated that the sample had typical amorphous structure.

3.3. Optical properties

The transmittance of the films measured by FTIR were lower than 70% in the region of 2.5 to 25 μm, as depicted in Fig. 6(a), where the peak centered at 4 μm inferred samples owning dominant aromatic rings or olefinic chain and the peak centered at 15 μm is characteristic peak of CO_2 from atmosphere [2,41]. Different from monotonic structural evolution of a-C films with deposition temperature, the transmittance first decreased to its minimum value lower than 40% at 100 °C, then rose again with further increasing deposition temperature up to 400 °C. Similar phenomenon was also observed by UV–visible spectrophotometer from 0.2 to 1.5 μm, as shown in Fig. 6(b), and all the a-C films exhibited extremely low transmittance, lower than 5%, in the wavelength range of 200 to 750 nm which proved that these films had

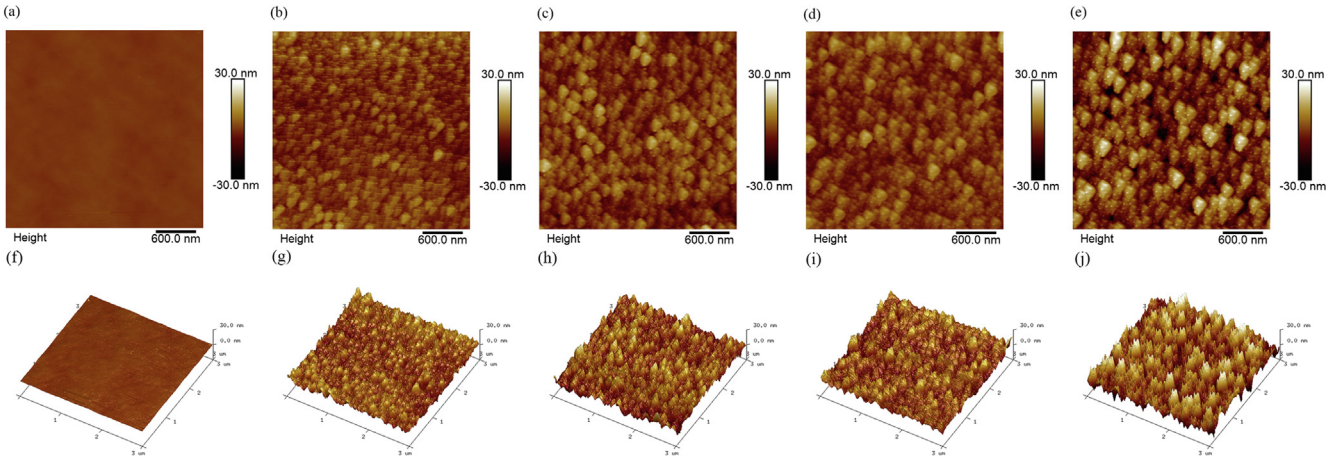

Fig. 2. The tapping mode 2D-AFM images (a), (b), (c), (d), (e) and the corresponding 3D-AFM images (f), (g), (h), (i), (j) of the films deposited at 30 °C, 100 °C, 200 °C, 300 °C and 400 °C.

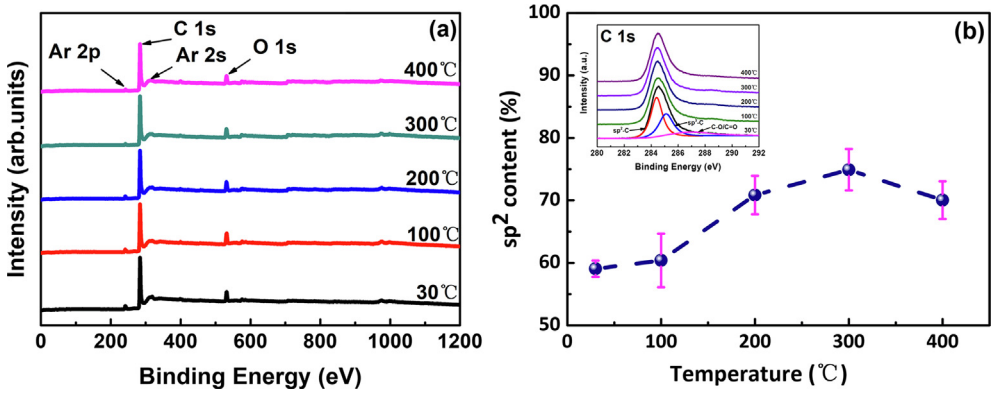

Fig. 3. (a) XPS spectra of the a-C films at various deposition temperatures; (b) The change of sp^2 content of a-C films with the variation of temperature, and the insert figure exhibits all C 1s peaks of the a-C films.

very strong light absorption properties in the range of ultraviolet and visible wavelength.

Tauc model is one of the most widespread used model to determine the optical properties of a-C films, and the band gap energy E_{opt} can be calculated from $E(\varepsilon)^{1/2}$ as function of the incident energy E [42]. The Tauc optical gap associated with the thin films is determined through an extrapolation of the linear trend observed in the spectral dependence of $(\alpha h\nu)^{1/2}$ over a limited range of photon energies $h\nu$. The Tauc optical gap is defined as occurring at the intercept of this linear extrapolation with the abscissa axis [43,44]. The absorption coefficient α near the band edge in a-C films shows an exponential dependence upon photon energy usually obeying the empirical relation,

$$\alpha = A(h\nu - E_{opt})^n/(h\nu) \quad (1)$$

where A is the band edge parameter and n is a number characterizing the transition process which may take values 1/2, 1, 3/2 or 2, depending upon the nature of the electronic transitions responsible for the absorption [45,46]. For a-C films, optical transitions are described to a first approximation by non-direct transitions with no conservation of electronic momentum, for allowed indirect transitions n = 2 [24]. Thus, the optical gaps for both indirect transitions could be determined by the extrapolation to zero of the linear regions in the plot of $(\alpha h\nu)^{1/2}$ vs. photon energy $h\nu$, as shown in Fig. 6(c).

Fig. 6(d) indicated that the optical bandgap first increased to its maximum value 0.45 eV at 100 ˚C, and then declined to 0.26 eV at 400 ˚C with further increase of the deposition temperature. This change of the Tauc optical gap in a-C films had been attributed to a number of factors, such as thickness of the films, contents and size of sp^2 clusters and disordering of π bond [44].

3.4. Electrical properties

I-V feature of a-C films was investigated by Hall-effect measurement, as shown in Fig. 7(a), all I-V plots exhibited a linear dependence, suggesting typical ohmic behavior. And the resistivity R of the a-C films can be calculated from the I-V plots as displayed in Fig. 7(b), the R first decreased from its maximum value 1.589×10^{-2} Ω·cm at 30 ˚C to its minimum value 2.191×10^{-3} Ω·cm at 100 ˚C, then increased monotonically with increasing deposition temperature to 400 ˚C.

Fig. 8 shows I-V plots of the films in the temperature range of 5 to 350 K, for the sample deposited at 30 ˚C, its I-V plots in the range of 5 to 50 K were not present here, since its resistance exceeded the upper limit of the instrument test range. Overall, all the samples displayed typical linear resistance characteristics in the range of 5–350 K, and their I-V plots were highly repeatable both during heating and cooling process, besides, the corresponding voltage of each sample decreased with increasing temperature at a certain excitation, which indicated the typical semiconductor behavior of the a-C films. In addition, at a certain test temperature, the sample deposited at 100 ˚C exhibited the lowest voltage compared with other samples at the same excitation, which matched well with the previous Hall-effect measurement.

In order to further explore its electrical properties, temperature dependence of dark resistivity (R-T) of the samples deposited at various temperatures was investigated, as shown in Fig. 9(a) and (b). In this test temperature range from 5 K to 350 K, the sample with a larger resistivity at room temperature also exhibited worse conductivity. Besides, the resistivity of all samples monotonically decreased with increasing temperature, and the sample with a larger resistivity varied more evidently. For example, the resistivity of sample deposited at 30 ˚C decreased 2 orders from 6.49 Ω·cm at 50 K to 5.57×10^{-2} Ω·cm at 350 K, while, that of sample deposited at 100 ˚C just decreased slightly

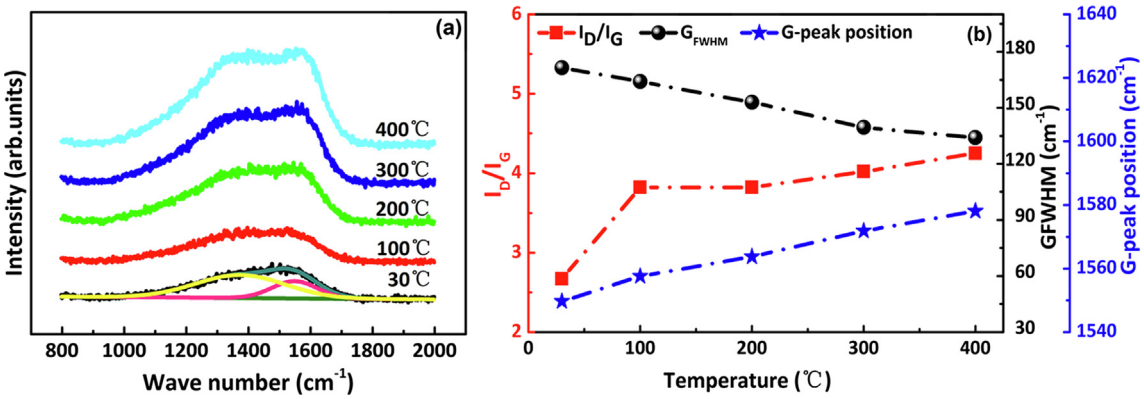

Fig. 4. (a) Raman spectra; (b) The corresponding fitting results of a-C films deposited at different temperature.

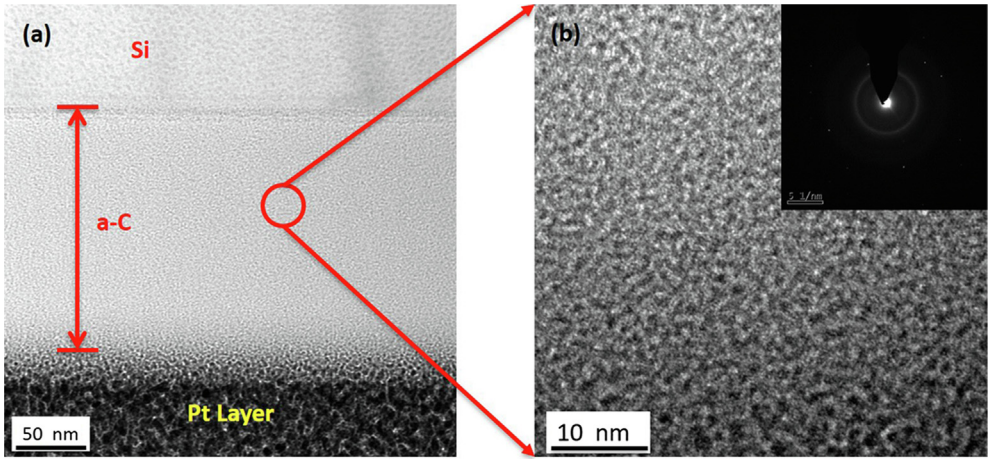

Fig. 5. (a) Cross-sectional TEM image, (b) HRTEM image and corresponding SAED of a-C film deposited at 100 °C.

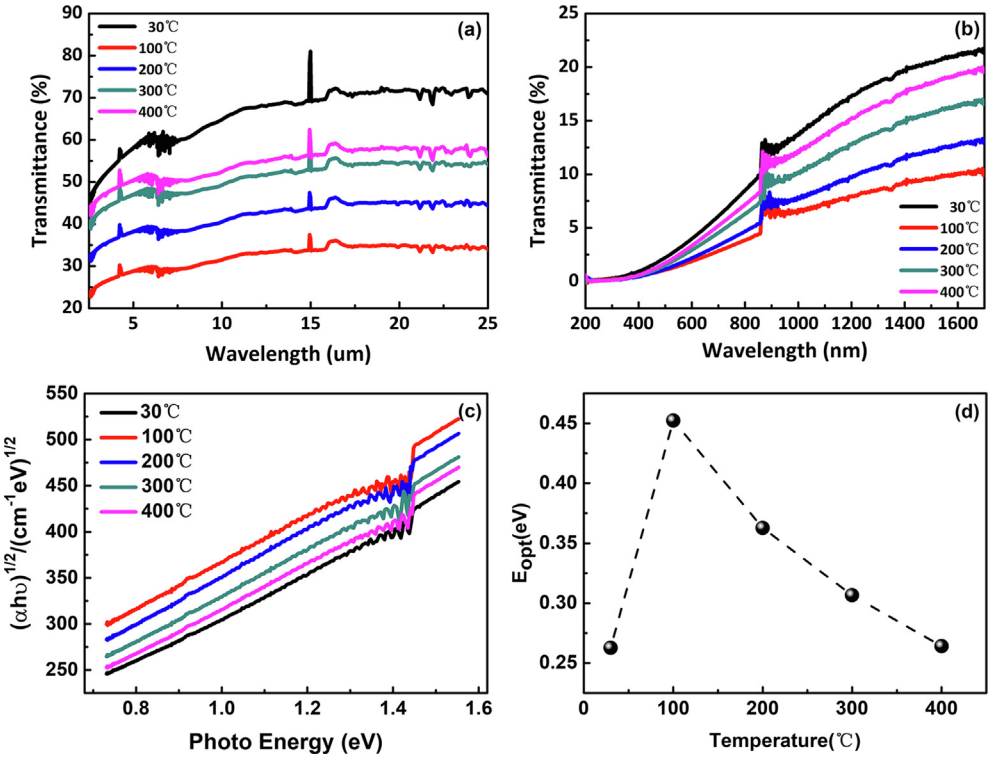

Fig. 6. Transmittances of the deposited a-C films with the variation of temperatures in different wavelength range (a) 2.5–25 μm and (b) 0.2–1.5 μm; (c) Typical Tauc plot to determine (d) optical bandgap of a-C films at various temperatures.

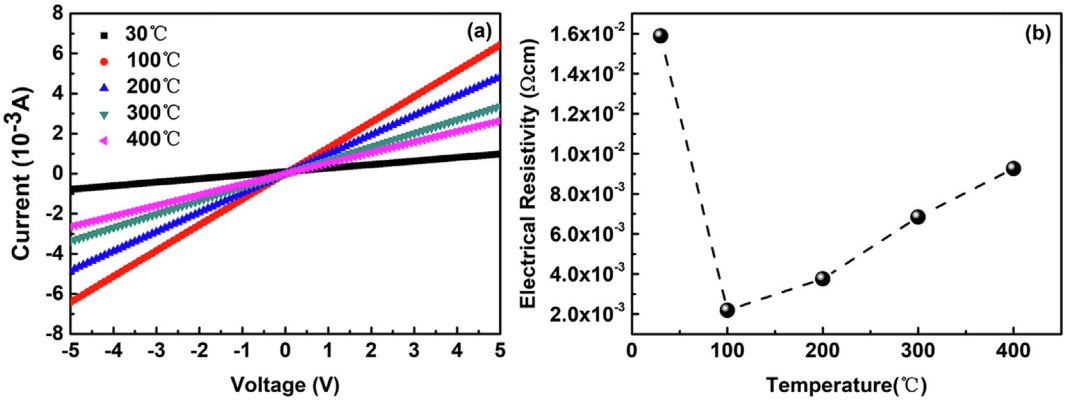

Fig. 7. (a) I-V characteristic plot and (b) electrical resistivity of the a-C film deposited at different temperature.

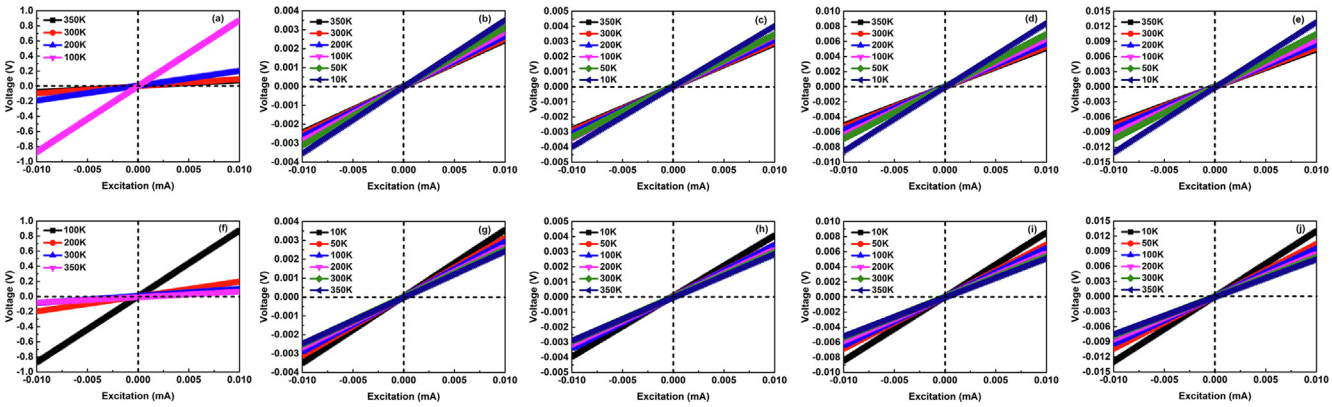

Fig. 8. I-V plots during cooling process (a), (b), (c), (d), (e) and heating process (f), (g), (h), (i), (j) of the a-C films deposited at 30 °C, 100 °C, 200 °C, 300 °C and 400 °C.

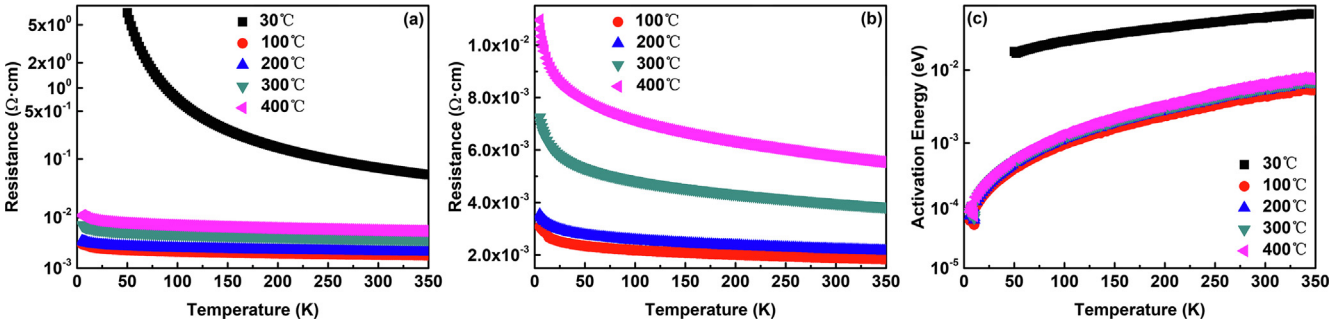

Fig. 9. (a) R-T behaviors of a-C films deposited at various temperature and (b) the enlarged figure with resistivity range from 0 to 0.012 Ω·cm, (c) variation of activation energy with temperature.

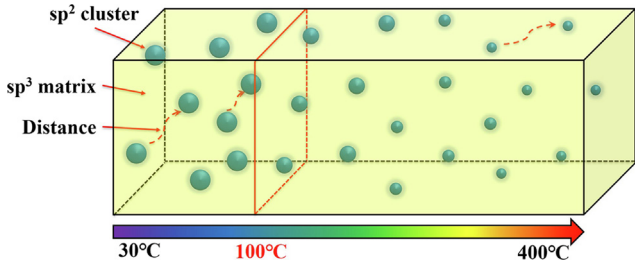

Fig. 10. Schematic diagram of transport mechanism in a-C films deposited in different temperature.

from 3.08×10^{-3} Ω·cm at 5 K to 1.84×10^{-3} Ω·cm at 350 K.

In general, the activation energy (E_{act}) is used to characterize the temperature dependence of conductivity in a-C films, which can be calculated from the arrhenius law, according to the following formula,

$$E_{act} = -k[d\ln(\sigma)/d(1/T)] \quad (2)$$

where σ is the conductivity of a-C films, that is the multiplicative inverse of resistivity, k is Boltzmann constant, and T is test temperature [18,48,49]. As shown in Fig. 9(c), the sample with a larger resistivity also exhibited a higher E_{act}, in addition, all E_{act} of the samples increased mildly with increasing temperature. For instance, from 0.011 eV at 50 K to 0.048 eV at 350 K for the sample deposited at room temperature and from 4.3×10^{-6} eV at 5 K to 5.5×10^{-3} eV at 350 K for the sample deposited at 100 °C, respectively [18,49], which was usually explained from the broad distribution of band tail states in the a-C films [18].

3.5. Discussion

From the optical and electrical properties of a-C films, their transmittance, optical bandgap, resistivity and activation energy exhibited similar tendency with increasing deposition temperature, which can be explained from the evolution of sp^2/sp^3 ratio and sp^2 cluster in the a-C films. Generally, the transmittance and optical bandgap of a-C films decrease with increasing the sp^2 content and size of sp^2 cluster at relatively low total disordering level [2,42,47]. Namely, the sp^2 content and size of sp^2 cluster determined the transmittance and optical bandgap simultaneously.

According to XPS, Raman and TEM, it was safe to deduce that, by changing the deposition temperature from 30 °C to 400 °C, the structure of a-C films became much more order, the sp^2 content of the films increased; in addition, it was proved that all the a-C films were in the transitional stage from amorphous carbon to nc-G; meanwhile, it might be interpreted that all the sp^2 clusters belonged same type since the oxygen content of all the a-C films was very low [15,50]. In general, it could be considered that the size of sp^2 clusters decreased with deposition temperature increasing, considering the theoretical model and the variation of photoelectric performance synthetically [31,40].

In this case, as deposition temperature increased to 100 °C, the increase of sp^2 contents could be the main factor to cause the decrease of transmittance and optical bandgap, since bond energy of sp^2–C is closed to Fermi level which had been proved by amount of computational study [13–15]; however, further increase the deposition temperature to 400 °C, the smaller size of sp^2 cluster resulted in the increase of transmittance and optical bandgap, which is the main factor to determine π band gap [13]. Similarly, the sp^2 content and size of sp^2 cluster can also decide the electrical properties of a-C films, by changing transition distances of electrons between clusters [11,12]. When deposition temperature was below 100 °C, the increase in sp^2 contents was the main reason to cause lower activation energy and reduced resistivity, at elevated temperature, smaller size of sp^2 clusters caused higher activation energy and larger band gap in this relatively stable sp^2 content range, as shown in Fig. 10.

4. Conclusion

In summary, by increasing deposition temperature from 30 ˚C to 400 ˚C, a-C films with higher sp^2 content and smaller size sp^2 cluster can be obtained. As the deposition temperature was below 100 ˚C, both transmittance and resistivity of a-C films decreased with increasing temperature, which can be explained from the increase of sp^2 of a-C films. As the deposition temperature increased from 100 ˚C to 400 ˚C, both transmittance and resistivity increased with increasing temperature, which was lied on the smaller size of sp^2 clusters. As a result, this study can provide a route to tune opto-electrical properties of a-C films for its application in amorphous carbon-based optoelectronic devices.

Acknowledgements

This work was financial supported by the National Natural Science Foundation of China (51602319, 11705258), Ningbo Science and Technology Innovation Project (2018B10014) and Natural Science Foundation of Ningbo (2018A610080).

References

[1] H.Y. Ueng, C.T. Guo, K.H. Dittrich, Development of a hybrid coating process for deposition of diamond, Surf. Coat. Technol. 200 (9) (2006) 2900–2908.
[2] J. Robertson, Diamond-like amorphous carbon, Mater. Sci. Eng. 37 (4–6) (2002) 129–281.
[3] K. Bewilogua, D. Hofmann, History of diamond-like carbon films - From first experiments to worldwide applications, Surf. Coat. Technol. 242 (2014) 214–225.
[4] M. Moseler, P. Gumbsch, C. Casiraghi, A.C. Ferrari, J. Robertson, The ultrasmoothness of diamond-like carbon surfaces, Science 309 (5740) (2005) 1545–1548.
[5] V.L. Deringer, M.A. Caro, R. Jana, A. Aarva, S.R. Elliott, T. Laurila, G. Csanyi, L. Pastewka, Computational surface chemistry of tetrahedral amorphous carbon by combining machine learning and density functional theory, Chem. Mater. 30 (21) (2018) 7438–7445.
[6] A. Grill, Electrical and optical properties of diamond-like carbon, Thin Solid Films 355–356 (14) (1999) 189–193.
[7] P. Guo, R. Chen, L. Sun, X. Li, P. Ke, Q. Xue, A. Wang, Bulk-limited electrical behaviors in metal/hydrogenated diamond-like carbon/metal devices, Appl. Phys. Lett. 112 (2018) 033502.
[8] F. Stock, F. Antoni, L. Diebold, UV laser annealing of Diamond-Like Carbon layers obtained by Pulsed Laser Deposition for optical and photovoltaic applications, Appl. Surf. Sci. 464 (2019) 562–566.
[9] D. Chen, M. Hofmann, H. Yao, Lateral two-dimensional material heterojunction photodetectors with ultrahigh speed and detectivity, ACS Appl. Mat. Interfaces 11 (6) (2019) 6384–6388.
[10] Y. Zhang, X. Wang, J. Zheng, Facile synthesis of high-surface vanadium nitride/vanadium sesquioxide/amorphous carbon composite with porous structures as electrode materials for high performance symmetric supercapacitors, Appl. Surf. Sci. 471 (2019) 842–851.
[11] H.Y. Dai, X.R. Cheng, C.F. Wang, Y.C. Xue, Z.P. Chen, Structural, optical and electrical properties of amorphous carbon films deposited by pulsed unbalanced magnetron sputtering, Optik 126 (7–8) (2015) 861–864.
[12] E. Mohagheghpour, M. Rajabi, R. Gholamipour, M.M. Larijani, S. Sheibani, Correlation study of structural, optical and electrical properties of amorphous carbon thin films prepared by ion beam sputtering deposition technique, Appl. Surf. Sci. 360 (2016) 52–58.
[13] M.A. Caro, R. Zoubkoff, O. Lopez-Acevedo, T. Laurila, Atomic and electronic structure of tetrahedral amorphous carbon surfaces from density functional theory: Properties and simulation strategies, Carbon 77 (2014) 1168–1182.
[14] T. Laurila, S. Sainio, M.A. Caro, Hybrid carbon based nanomaterials for electrochemical detection of biomolecules, Prog. Mater. Sci. 88 (2017) 499–594.
[15] M.A. Caro, A. Aarva, V.L. Deringer, G. Csanyi, T. Laurila, Reactivity of amorphous carbon surfaces: rationalizing the role of structural motifs in functionalization using machine learning, Chem. Mater. 30 (21) (2018) 7438–7445.
[16] J.Y. Sze, B.K. Tay, D. Sheeja, S.P. Lau, Y.Q. Fu, D.H.C. Chua, W.I. Milne, Optical and electrical properties of amorphous carbon films deposited using filtered cathodic vacuum arc with pulse biasing, Thin Solid Films 447 (3) (2004) 148–152.
[17] X. Ma, P. Guo, X. Tong, Y. Zhao, Q. Zhang, P. Ke, A. Wang*, Piezoresistive behavior of amorphous carbon films for high performance MEMS force sensors, Appl. Phys. Lett. 114 (2019) 253502 1-4.
[18] S. Bhattacharyya, S.R.P. Silva, Transport properties of low-dimensional amorphous carbon films, Thin Solid Films 482 (1–2) (2005) 94–98.
[19] X. Zuo, P. Ke, R. Chen, X. Li, M. Odén, A. Wang, Discharge state transition and cathode fall thickness evolution during chromium HiPIMS discharge, Phys. Plasmas 24 (8) (2017) 083507.
[20] Y. Taki, O. Takai, XPS structural characterization of hydrogenated amorphous carbon thin films prepared by shielded arc ion planting, Thin Solid Films 316 (1–2) (1998) 45–50.
[21] J. Díaz, G. Paolicelli, S. Ferrer, F. Comin, Separation of the sp^3 and sp^2 components in the C1s photoemission spectra of amorphous carbon films, Phys. Rev. B 54 (11) (1996) 8064–8069.
[22] P. Merel, M. Tabbal, M. Chaker, S. Moisa, J. Margot, Direct evaluation of the sp^3 content in diamond-like-carbon films by XPS, Appl. Surf. Sci. 136 (1998) 105–110.
[23] M.E. Sanchez-Vergara, J.C. Alonso-Huitron, A. Rodriguez-Gomez, J.N. Reider-Burstin, Determination of the optical GAP in thin films of amorphous dilithium phthalocyanine using the Tauc and Cody models, Molecules 17 (9) (2012) 10–13.
[24] I. Alexandrou, A.J. Papworth, C.J. Kiely, G.A.J. Amaratunga, L.M. Brown, Calculation of the bandgap and of the type of interband transitions in tetrahedral amorphous carbon using electron energy loss spectroscopy, Diamond Relat. Mater. 13 (4–8) (2004) 1408–1411.
[25] E. Mounier, F. Bertin, M. Adamik, Y. Pauleau, P.B. Barna, Effect of the substrate temperature on the physical characteristics of amorphous carbon films deposited by dc magnetron sputtering, Diamond Relat. Mater. 12 (5) (1996) 1509–1515.
[26] M. Shinohara, K. Cho, Y. Matsuda, T. Inayoshi, H. Kawazoe, H. Fujiyama, T. Nakatani, Substrate temperature effects on amorphous carbon film growth, investigated by infrared spectroscopy in multiple internal reflection geometry, J. Vac. Sci. Technol. A 27 (4) (2009) 813–817.
[27] M.R. Shen, H. Wang, Z.Y. Ning, Y. Chao, Z.X. Ren, A model for the simultaneous growth of amorphous carbon and diamond film, J. Phys. Condens. Matter 9 (14) (1997) 2981–2986.
[28] Z. Zhai, H. Shen, J. Chen, Y. Jiang, Q. Tang, Investigation of substrate temperature and cooling method on the properties of amorphous carbon films by hot-filament CVD with acetylene, Carbon 117 (2017) 322–330.
[29] S. Nakao, K. Yukimura, S. Nakano, H. Ogiso, DLC coating by HiPIMS: the influence of substrate bias voltage, IEEE Trans. Plasma Sci. 41 (8) (2013) 1819–1829.
[30] P. Guo, X. Li, L. Sun, R. Chen, P. Ke, A. Wang, Stress reduction mechanism of diamond-like carbon films incorporated with different Cu contents, Thin Solid Films (2017).
[31] J. Koskinen, J.P. Hirvonen, J. Keranen, Effect of deposition temperature and growth rate on the bond structure of hydrogen free carbon films, J. Appl. Phys. 84 (1) (1998) 648–650.
[32] W. Pfleging, R. Kohler, M. Torge, V. Trouillet, F. Danneil, M. Stüber, Control of wettability of hydrogenated amorphous carbon thin films by laser-assisted micro- and nanostructuring, Appl. Surf. Sci. 257 (2011) 7907–7912.
[33] A.M. Ito, A. Takayama, S. Saito, H. Nakamura, Formation and classification of amorphous carbon by molecular dynamics simulation, Jpn. J. Appl. Phys. 45 (29) (2006) L755–L757.
[34] J.R. Andrea Carlo Ferrari, Raman of DLC and carbon diamond, Phil. Trans. R. Soc. Lond. A 362 (2004) 2477–2512.
[35] A.C. Ferrari, J. Robertson, Interpretation of Raman spectra of disordered and amorphous carbon, Phys. Rev. B 61 (20) (2000) 14095–14107.
[36] H.X. Li, T. Xu, J.M. Chen, H.D. Zhou, H.W. Liu, The effect of applied dc bias voltage on the properties of a-C : H films prepared in a dual dc-rf plasma system, Appl. Surf. Sci. 227 (2004) 364–372.
[37] P.K. Chu, L. Li, Characterization of amorphous and nanocrystalline carbon films, Mater. Chem. Phys. 96 (2006) 253–277.
[38] C. Casiraghi, A.C. Ferrari, J. Robertson, Raman spectroscopy of hydrogenated amorphous carbon, Phys. Rev. B 72 (8) (2005).
[39] C. Thomsen, S. Reich, Double Resonant Raman Scattering in Graphite Phys, Rev. Lett. 85 (2000) 5214.
[40] F. Tuinstra, J.L. Koening, Raman spectrum of graphite, J. Chem. Phys. 53 (1970) 1126.
[41] Y. Wang, K. Gao, Q. Wang, J. Zhang, The correlation between nano-hardness and elasticity and fullerene-like clusters in hydrogenated amorphous carbon films, Chem. Phys. Lett. 692 (2018) 258–263.
[42] N. Laidani, R. Bartali, G. Gottardi, M. Anderle, P. Cheyssac, Optical absorption parameters of amorphous carbon films from forouhi-bloomer and tauc-lorentz models: A comparative study, J. Phys. Condens. Matter. 20 (2008).
[43] S.K. O'Learly, P.K. Lim, On determining the optical GAP associated with an amorphous semiconductor: A generalization of the tauc model, Solid State Commun. 104 (1997) 17–21.
[44] T.M. Mok, S.K. O'Leary, The dependence of the Tauc and Cody optical gaps associated with hydrogenated amorphous silicon on the film thickness: αl Experimental limitations and the impact of curvature in the Tauc and Cody plots, J. Appl. Phys. 102 (2007) 113525 1–113525:9.
[45] F. Urbach, The long-wavelength edge of photographic sensitivity and of the electronic absorption of solids, Phys. Rev. 92 (1953) 1324.
[46] M.E. Sanchez-Vergara, J.C. Alonso-Huitron, A. Rodriguez-Gomez, J.N. Reider-Burstin, Determination of the optical GAP in thin films of amorphous dilithium phthalocyanine using the Tauc and Cody models, Molecules 17 (9) (2012) 10000–10013.
[47] Z. Zhai, H. Shen, J. Chen, Y. Jiang, Q. Tang, Investigation of substrate temperature and cooling method on the properties of amorphous carbon films by hot-filament CVD with acetylene, Carbon 117 (2017) 696–701.
[48] S. Bhattacharyya, Observation of delocalized transport and low-dimensionality effects in disordered carbon thin films, Appl. Phys. Lett. 91 (14) (2007) 142116.
[49] M. Koós, S.H.S. Moustafa, E. Szilágyi, I. Pócsik, Non-Arrhenius temperature dependence of direct-current conductivity in amorphous carbon (a-C:H) above room temperature, Diamond Relat. Mater. 8 (1999) 1919–1926.
[50] M.A. Caro, V.L. Deringer, J. Koskinen, T. Laurila, G. Csanyi, Growth Mechanism and Origin of High sp^3 Content in Tetrahedral Amorphous Carbon, Phys. Rev. Lett. 120 (16) (2018) 166101.